NUREG/CR-3804 Vol. I
ANL-84-35 Vol. I

NUREG/CR-3804 Vol. I
ANL-84-35 Vol. I

PHYSICS OF REACTOR SAFETY

Quarterly Report
January – March 1984

ARGONNE NATIONAL LABORATORY, ARGONNE, ILLINOIS
Operated by THE UNIVERSITY OF CHICAGO

Prepared for the Office of Nuclear Regulatory Research
U. S. NUCLEAR REGULATORY COMMISSION
under Interagency Agreement DOE 40-550-75

Argonne National Laboratory, with facilities in the states of Illinois and Idaho, is owned by the United States government, and operated by The University of Chicago under the provisions of a contract with the Department of Energy.

Available from

GPO Sales Program
Division of Technical Information and Document Control
U. S. Nuclear Regulatory Commission
Washington, D.C. 20555

and

National Technical Information Service
Springfield, Virginia 22161

NUREG/CR-3804 Vol. I
ANL-84-35 Vol. I

(Distribution
Code: R7)

ARGONNE NATIONAL LABORATORY
9700 South Cass Avenue
Argonne, Illinois 60439

PHYSICS OF REACTOR SAFETY

Quarterly Report
January—March 1984

Applied Physics Division
Components Technology Division

May 1984

Previous reports in this series

ANL-83-11 (I)	January—March 1983
ANL-83-11 (II)	April—June 1983
ANL-83-11 (III)	July—September 1983
ANL-83-11 (IV)	October—December 1983

Prepared for the Division of Accident Evaluation
Office of Nuclear Regulatory Research
U. S. Nuclear Regulatory Commission
Washington, D. C. 20555
Under Interagency Agreement DOE 40-550-75

NRC FIN Nos. A2015 and A2045

PHYSICS OF REACTOR SAFETY

Quarterly Report
January-March 1984

ABSTRACT

This Quarterly progress report summarizes work done during the months of January-March 1984 in Argonne National Laboratory's Applied Physics and Components Technology Divisions for the Division of Reactor Safety Research of the U.S. Nuclear Regulatory Commission. The work in the Applied Physics Division includes reports on reactor safety modeling and assessment by members of the Reactor Safety Appraisals Section. Work on reactor core thermal-hydraulics is performed in ANL's Components Technology Division, emphasizing 3-dimensional code development for LMFBR accidents under natural convection conditions. An executive summary is provided including a statement of the findings and recommendations of the report.

FIN No.	Title
A2015	Reactor Safety Modeling and Assessment
A2045	3-D Time-dependent Code Development

TABLE OF CONTENTS

LIST OF FIGURES

LIST OF TABLES

EXECUTIVE SUMMARY

The FPIN2 code is being used for parametric studies of LMFBR oxide fuel pin failure. An important feature in FPIN2 is the ability to calculate the restraint on axial fuel expansion due to fuel/cladding binding when the gap between the fuel and cladding is closed. Previous calculations with FPIN1 and SAS/EPIC, which did not include this effect, have been felt to overestimate axial expansion of the molten fuel cavity which is a source of pressurization affecting fuel pin failure. Indeed, FPIN2 calculations of a TOP with the fuel/cladding gap closed at steady state show a 0.5% axial expansion of the cavity and a total cavity volume decrease of 3% rather than the larger axial expansions and total cavity volume increases calculated by SAS/EPIC (1.5% axial, 6% total) and FPIN1 (7-8% axial, 10% total). These differences in cavity expansion could be significant in the determination of fuel pin failure time under TOP conditions.

The BIFLO code for analysis of two-dimensional sodium boiling in a fuel assembly has been modified to implement a more implicit numerical formulation, an equation of state for pure sodium vapor, and lateral heat conduction between sodium flow channels. The modified code is being used to perform a posttest analysis of a flow coastdown performed in a 15-pin bundle in the OPERA Facility. A one-dimensional simulation through the time of inlet flow reversal has been completed; stability problems are being encountered shortly after boiling in the two-dimensional simulation.

In the area of single-phase COMMIX development, the following four major efforts were made this quarter. They are:

- Initiation of free surface boundary option.
- Implementation and partial validation of turbulence model for low Reynolds number flow.
- Interfacing of COMMIX-1B by establishing a master file and rerunning four test problems.
- Implementation of second fluid option with a desire to enhance COMMIX applicability to the analysis of Direct Reactor Auxiliary Cooling System (DRACS).

In the COMMIX-2 development work, we have continued effort to simulate German seven-pin problem with thermal-equilibrium model with slip. The results of simulation are in good agreement with most parts of the transient except during the period (after power switch-off) when condensation of vapor dominates. Further investigation of this problem suggested several modifications:

- Different heat transfer correlation to account for the increase in heat transfer due to liquid coolant film at the structure.
- Use of extrapolated value of velocity at the phase boundary for convective terms instead of using pure upwind differencing scheme.

- To reduce the energy imbalance and increase the convergence rate, we have added a term (that goes to zero when the convergence is achieved) on both sides of the difference equation to increase the diagonal dominance to the matrix of coefficients.

These modifications have improved the results but the problem is not completely resolved. Further investigations are being made.

In the area of two-fluid-model COMMIX-2 development, formulations have been completed, subroutines are written, and debugging has started.

I. REACTOR SAFETY MODELING AND ASSESSMENT

(A2015)

A. Fuel Pin Failure Studies (H. H. Hummel)

The FPIN2 code has been made available to us by the developers and is being used in parametric studies of pin failure in LMFBR oxide fuel. This code represents a considerable advance over FPIN1 in that it uses an improved numerical procedure involving use of finite elements. It also models crack volume, which FPIN1 did not. A further advance is that restraint of axial expansion of fuel by binding to clad when the fuel/clad gap is closed is an available option. The code is still rather expensive to run but is practical to use with judicious choice of computing priority.

The FPIN codes are of particular interest in that they are the only ones available to us that model fuel stress relaxation in detail. LAFM has an approximate treatment of stress relaxation involving use of a softening temperature. The DEFORM-III module of SAS4A currently does not have any treatment of fuel stress relaxation. An approximate model for this was originally included, but it proved unsuccessful and was removed. FPIN2 will be quite useful in judging the importance of modeling fuel stress relaxation and the validity of approximate treatments of it.

A sealed cavity model is used to evaluate burst failure of clad in the FPIN codes, in LAFM, and in the SAS codes, including SAS/EPIC. Definitions of the cavity boundary range from the point at which the fuel attains its solidus temperature to that at which melting is complete. Assuming 0.50 melt fraction at the cavity boundary is typical. In the FPIN codes the fuel solidus temperature is used. Because the validity of assuming a sealed cavity in a slow TOP seemed to us to be open to question, in SAS/EPIC uniform pressurization of the whole pin in the core region is also an option. A problem relating to the cavity model we have been concerned with for some time is the effect of fuel pin mechanics on the cavity volume. Because we did not have a fuel dynamics calculations available in SAS/EPIC, we assumed that the fuel at the cavity boundary was displaced during the transient from the original steady-state position according to free thermal expansion. This typically led to a cavity expansion of about 6%, about 4.5% radial and 1.5% axial.[1] FPIN1 tended to give about the same or slightly larger cavity expansions, up to about 10%, but with all but 2 or 3% being axial expansion.[2] It was always felt, however, that this axial fuel expansion was too large because the restraining effect of clad was not taken into account. First results from FPIN2 for TOP cases with fuel/clad gap assumed closed in steady state indicate that this is indeed the case. Axial fuel expansion calculated assuming fuel/clad binding when the gap is closed and with the plane strain approximation always used in fuel modeling codes amounts to only about 0.5%. Radial cavity expansion up to the time of runaway plastic clad strain is actually negative so that the cavity volume change from fuel displacement is about -3% at the time burst failure conditions are attained. This difference in cavity volume at failure from fuel displacement from previous results can be significant in determining failure time as it is about half the fuel volume increase from steady state to melting and is of the same order as typical fuel porosity. Different results may be obtained for LOF-TOP cases because of the possibility of opening of the fuel/clad gap.

Results from FPIN2 are found to be quite independent of time step size, which was not the case for FPIN1, and is reassuring with regard to the accuracy of the calculations. The balance between time step size and iterations required per time step seems to be such that it is advantageous to use time steps as large as possible without having the calculations fail to converge.

B. BIFLO Code Development (P. L. Garner)

The BIFLO code is being developed for two-dimensional analysis of sodium boiling in a fuel assembly within the context of a whole-core reactor accident analysis calculation. Work has continued on the recent code revisions which were made to implement a more implicit formulation of the equations, an equation of state for pure vapor, and lateral conduction of heat between sodium flow channels. Calculations are being performed for loss of flow and total inlet flow area blockage cases using both one- and two-dimensional fuel assembly models to assess the new modeling as it is developed.

A posttest analysis of a sodium flow coastdown experiment, which was performed in a 15-pin triangular bundle in the OPERA Facility at ANL, has continued. In the experiment[3], localized boiling occurred 9.4 s after the start of the flow reduction; the localized boiling propagated to involve the full bundle flow area over the next 1.6 s. Initial reversal of the inlet flow occurred 12.0 s after the start of the flow reduction; thereafter, the inlet flow oscillated at a frequency of ~2 Hz.

Difficulty has been experienced in trying to develop a characterization of the OPERA Facility's hydraulics (especially for the region between the sodium supply vessel and the inlet to the heated pin bundle) in a form suitable for use in BIFLO. This relationship must be properly modeled since the time history of the mass flow rate and the pressures are important factors in determining the boiling initiation and progression; a simulation of the test needs to be driven by measured pressures which lead to the calculation of the measured flow rate (rather than being driven directly by the measured flow rate). The pressure and flow rate data measured in the Facility for a series of steady-state runs have been obtained from the experimenter in order to aid in this analysis. The data are, unfortunately, rather scattered when converted to mass flow versus pressure drop, which tends to amplify errors in absolute pressure measurement at low flow rates. Although the scatter in the data precludes a definitive analysis, a hydraulics characterization has been developed which will allow calculations to proceed.

A one-dimensional BIFLO calculation of this experiment has been completed which showed sodium boiling at 11.8 s (which is, as is to be expected from a one-dimensional model, too late relative to the experiment), inlet flow reversal at 12.5 s (which is later than observed in the experiment but is consistent with the trend observed in pretest calculations[4] that a one-dimensional calculation overestimates the time of inlet flow reversal), and subsequent oscillations of the inlet flow at a frequency of 5 to 9 Hz. Although this one-dimensional calculation is not a particularly good representation of the two-dimensional behavior in the experiment, the calculation is useful for comparison with one-dimensional calculations being peformed by others and as a base against which two-dimensional calculations may be compared. Stability problems with the lateral momentum equation have arisen during the process of performing a two-dimensional analysis of the experiment using BIFLO.

The calculation has been stabilized prior to boiling by adding an extra iterative sequence which performs a simultaneous solution of the axial momentum, lateral momentum and state equations. Although the technique used is not particularly efficient and does not provide sufficient stability after boiling begins, the modification has allowed a two-dimensional analysis of the experiment to proceed. The two-dimensional BIFLO calculation showed boiling initiation at 9.5 s after the start of the flow reduction, which is in good agreement with the experiment result. The calculation became unstable over the next 0.1 s; various methods for restoring stability are being examined.

II. THREE-DIMENSIONAL CODE DEVELOPMENT FOR CORE THERMAL-HYDRAULIC ANALYSIS OF LMFBR ACCIDENTS UNDER NATURAL CONVECTION CONDITIONS

A2045

A. INTRODUCTION

The objective of this program is to develop computer programs (COMMIX and BODYFIT) which can be used for either single-phase or two-phase thermal-hydraulic analysis of reactor components under normal and off-normal operating conditions, especially under natural circulation. The governing equations of conservation of mass, momentum, and energy are solved as a boundary value problem in space and as an initial value problem in time.

COMMIX is a three-dimensional, transient, compressible flow computer code for reactor thermal-hydraulic analysis. It is a component code and uses a porous medium formulation to permit analysis of a reactor component/multicomponent system, such as fuel assembly/assemblies, plenum, piping system, etc., or any combination of these components. The concept of volume porosity, surface permeability, and distributed resistance and heat source (or sink) is employed in the COMMIX code for quasi-continuum thermal-hydraulic analysis. It provides a greater range of applicability and an improved accuracy than subchannel analysis. By setting volume porosity and surface permeability equal to unity, and resistance equal to zero, the COMMIX code can equally handle continuum problems (reactor inlet or outlet plenum, etc.).

B. COMMIX-1A, COMMIX-1B, Single-Phase Code Development (M. Bottoni, F. F. Chen, H. N. Chi, T. Chiang, H. M. Domanus, R. C. Schmitt, W. T. Sha, V. L. Shah, and J. E. Sullivan)

B.1. Free Surface Boundary Option

We are starting to develop a "free surface boundary" option for COMMIX-1B. Several approaches that are reported in the literature have been examined.

The Lagrangian representation of the free surface has been ruled out on the ground that the constant deformation of the free boundary is not suitable for COMMIX.

The Marker-in-Cell[5] (MAC) procedure requires a lot of computer storage and is very sensitive to how the Marker's velocities are averaged. Furthermore, the Marker displacement, which traces the free surface movement, requires artificial (numerical) limitation to maintain a recognizable shape of the free surface. Such restriction may not suit the current fully-implicit framework of COMMIX-1B.

We have therefore, decided to develop a new scheme based on the volume of fluid[6] (VOF) approach. The new method to be developed will be fully-implicit and compatible with the COMMIX environment.

B.2 Turbulence Model for Low Reynolds Number Flow

Implementation of the low Reynolds number version of the 2-equation k-ε turbulence model into the COMMIX code has been completed. A new subroutine called TKDLOW has been introduced for the calculation of additional terms that arise in this model. A new variable called LOWREY is introduced to activate this model:

ITURKE = 12 and LOWREY = 0; High Reynolds number version of k-ε model

ITURKE = 12 and LOWREY = 1; Low Reynolds number version of k-ε model.

Details of the low Reynolds number version of the k-ε model were discused in the last quarterly report.

The results of an isothermal fluid in a circular duct at three different Reynolds numbers are presented here to demonstrate the capability of the low Reynolds version of the k-ε turbulence model. Due to axisymmetry, the flow is two-dimensional. A total of 500 cells (10 in the r-direction and 50 in the z-direction) were used to model the geometry.

Figure 1 shows the axial velocity profile at Z/D = 48.0 (Z being the axial distance and D being the pipe diameter) at Reynolds number equal to 1000. Since the Reynolds number is low and the flow is laminar, the results of using the high Reynolds number version of the k-ε model (called model-2) are not good, whereas the results of the low Reynolds number version of the k-ε model (model-1) are very good. The results of model-1 are very close to the results of using the laminar flow model. However, if the Reynolds number increases to 10000 (turbulent flow), the results of model-1 are not as good as model-2, but the difference is small. The results of axial velocity at Z/D = 40.5 are presented in Fig. 2. The axial velocity at Z/D = 40.5 for Re = 3.38×10^5 are presented in Fig. 3.

The results of model-2 are very close to the experimental results of Ref. 7, whereas the results of model-1 are not good anymore. The reason for the bad results of model-1 can be explained. Since the near wall logarithmic velocity profile is not used in model-1, the calculated turbulent viscosity near the wall is very small. Therefore, for the case of highly turbulent flow, wall functions similar to those used by the high Reynolds k-ε model are needed for model-1. Further studies of model-1 especially for the case of highly turbulent flow, will be done later. At the present, it is concluded that for the case of a natural circulation problem where flow may undergo transition from turbulent to laminar or vice versa, the use of the low Reynolds number version of the k-ε model is recommended. For the case of highly turbulent flow, we recommend that the popular high Reynolds number version of the k-ε model be used.

B.3 Interfacing of COMMIX-1B

In order to prepare the release of COMMIX-1B, version 1.0, a master file of COMMIX-1B must be established. Since previous implementation of new subroutines involving turbulence modeling and various skew-upwind

difference schemes were based on version 12.0 of COMMIX-1A, an interface procedure between these new subroutines and the latest version (12.7) of COMMIX-1A is required.

In the interface procedure, all the modifications to existing subroutines and new subroutines were carefully examined. Several typographical errors were found and corrected. At the present time, a total of 16 subroutines have been added to modify COMMIX-1A to COMMIX-1B; six for turbulence modeling and ten for skew-upwind and volume-weighted skew-upwind difference schemes.

A new master file for the COMMIX-1B has been established and is now ready for release. The output summary related to the turbulence modeling has been modified to provide a better output arrangement so that users can check and verify the turbulence related parameters very easily. To simplify the input, the input block for turbulence modeling has now been incorporated into the main input block - namelist data. This simplification is especially convenient in the re-start process.

Since the interfacing procedure required thorough testing, we ran four test problems to ensure that no coding errors have been introduced in the new COMMIX-1B master file. An isothermal developing turbulent flow problem was run to check the turbulence modeling section. To check various skew-upwind difference schemes in the cartesian coordinate, a thermal mixing problem of two fluids at different temperatures was used. The SAI thermal and fluid mixing test was used to check both the turbulence modeling and the volume-weighted skew-upwind difference scheme in the cartesian coordinate. Sample problem No. 2 of the released version of COMMIX-1A (CRBR outlet plenum simulation) was used to check the volume-weighted skew-upwind difference scheme in the cylindrical coordinate. A bug was discovered and corrected in the cylindrical portion of the volume-weighted skew-upwind difference scheme. The last test problem (CRBR outlet plenum simulation) is a first test problem for volume-weighted skew-upwind difference scheme in the cylindrical coordinate for which no comparisons with test data have been made.

B.4 Second Fluid Option

The other activity in the development of COMMIX-1B is the implementation of a second fluid option to analyze a system such as the Direct Reactor Auxiliary Cooling System (DRACS). At the present time, the physical properties of the second fluid are computed using the first order function of temperature, such as:

```
DENSITY = FCORO2 + FC1RO2*TC
VISCOSITY = FCOMU2 + FC1MU2*TC
CONDUCTIVITY = FC0K2 + FC1K2*TC
```

where TC is the temperature in degrees °C, and coefficients FCORO2, FC1RO2, FCOMU2, FC1MU2, FCOK2, and FC1K2 are constants.

With the current capability of COMMIX plus the second fluid option, the analysis of DRACS, such as Na/Nak or NaK/air heat exchangers, can be accomplished.

C. DEVELOPMENT OF COMMIX-2 (M. Bottoni, H. N. Chi, T. H. Chien, H. M. Domanus, R. W. Lyczkowski, C. C. Miao, W. T. Sha, and J. E. Sullivan)

C.1 Thermal Equilibrium Model with Slip

C.1.1 Properties of Water

A full set of functions for calculating the properties of water as a coolant has been made available, beyond those for sodium which are currently being used. These functions have been tabulated and checked with a program independent of COMMIX. For the sake of completeness a list of all functions used for calculating the coolant properties is given in Table 1.

C.1.2 Heat Transfer Coefficient

In the one-dimensional case, a full transient calculation, up to recondensation of the two-phase flow region after power switch-off, is now possible. The calculated development of the two-phase flow regime is in good agreement with the experimentally recorded data, as long as power is on. This implies that the vaporization dominates over the condensation of vapor in the uppermost cold part of the test section. After power switch-off, when the condensation of vapor dominates, the agreement is poor, because the condensation of vapor is not modeled correctly. The pin to coolant heat transfer coefficient is calculated with the same formula used for the single-phase flow region, which is not suitable in the boiling region.

The existence of a liquid coolant film at the structural and rod surfaces enhances the heat transfer as long as the surfaces are wetted. To simulate this behavior, an equivalent liquid film thickness δ has been calculated from the known value of liquid volume in a cell $((1 - \alpha)\gamma_v V_{cell}$, where γ_v is the volume porosity). The two-phase heat transfer coefficient is then calculated as

$$h = \frac{k}{\delta} \left(W/m^2 {}^0C\right) \tag{1}$$

where k is the liquid film thermal conductivity. When δ is smaller than a given minimum value (typically $\delta_{min} = 5 \times 10^{-6}$ m) dry-out is assumed and the heat-transfer coefficient drops to a very low value (typically 3000 $W/m^2 {}^0C$) which takes into account the residual heat transfer due to radiation. A model setting an upper bound to h, accounting for reaching the critical heat-flux conditions, should also be developed. For the time being, the condition $h \leq h_{max} = 3.5 \times 10^5$ $(W/m^2 {}^0C)$ is imposed.

C.1.3 Modification

Since July 1983, COMMIX-2 (thermal equilibrium model with slip) has been revised, restructured, and improved. For the sake of completeness, the most important of these program improvements are listed hereafter:

(a) As an alternative to the iterative Jacobi point-method of solution of the Poisson equations describing the pressure and enthalpy fields, a direct solution technique based on

matrix inversion has been made available. In more-dimensional cases, the matrix inversion is applicable in case of a definition domain consisting of a square array (2D), or consisting of a parallelepiped (3D). The gain in computer running time is by a factor of two to three in the two-dimensional case.

(b) The double-precision has always been used in COMMIX-2 calculations. When applying the matrix inversion method, the double precision is a compulsory requirement.

(c) The subroutines and functions needed for calculating the physical properties of the two-phase flow mixture have been completed and revised.

(d) All physical properties of the coolant (liquid, two-phase mixture, and vapor) are calculated only once per iteration loop and that too in only one driving subroutine (PHYHEM). Therefore, all physical properties are with reference to the same values of pressure and specific enthalpy.

(e) The terms describing the momentum-slip and the energy-slip for the cross-flow directions have been completely programmed, so that simulation of three-dimensional problems became possible.

(f) The term describing the sonic propagation has been linearized according to the formula:

$$\frac{\partial \rho}{\partial t} = \left(\frac{\partial \rho}{\partial h}\right)_p \frac{\partial h}{\partial t} + \left(\frac{\partial \rho}{\partial p}\right)_h \frac{\partial p}{\partial t} \,. \qquad (2)$$

(g) A new calculation of the two-phase heat transfer coefficient has been made, as explained above.

With these improvements, the bulk of the programming of COMMIX-2 (equilibrium model with slip) is basically considered complete, although refinements of detailed aspects (for instance, correlation for two-phase pressure drops) will be continued.

C.1.4 Simulation of German 7-Pin Experiment of the NSK Series

With the "Thermal Equilibrium with Slip" version now available, several one-dimensional and three-dimensional calculations have been made for the 7-2/16 experiment of the NSK series. No numerical difficulties were experienced in the 16-second transient simulation, i.e., up to the end of simulated pump coast-down accident (from 0 to 16 sec. of problem time; from 9.5 to 16 sec. in the two-phase flow region). The agreement between computed and experimental data is very good from boiling inception up to power switch-off (coolant temperatures, spreading of two-phase flow region, etc.). Calculated vapor velocities attained about 30-50 m/sec both in one- and three-dimensional simulations. After power switch-off, the recondensation of the boiling region does not appear to be simulated correctly because the

two-phase flow spreads unrealistically upwards. The 3D simulation is better than the 1D simulation.

During further investigation of problems of incorrect simulation of recondensation of boiling region, two reasons for some inconsistencies were identified.

(i) Use of Upwind Differences at Phase Boundaries

The reasons for the incorrect behavior appears to be due to the application of the upwind finite-difference scheme at the boundary between the two-phase and the single-phase flow regions. Let us assume, for instance, that in the one-dimensional simulation, the coolant flows in the upward direction. Then application of the upwind scheme to the lowermost mesh of the uppermost liquid slug implies that we are using a vapor velocity (from the uppermost mesh in the boiling region) to calculate a liquid mass flow. This produces an error of the order of magnitude of the slip ratio. Thus, the mass flow at the phase boundary is overestimated and forces an erroneous spreading of the two-phase flow region.

This problem, related to the use of upwind differencing, is very similar to the one that occurs when flow is sharply inclined to coordinate grid lines.

An attempt to resolve this difficulty has been made by computing the velocity at the phase boundary by extrapolating the liquid velocity in the adjacent slugs. This artifice works, and prevents the spreading upwards of the two-phase flow region, but introduces a local mass imbalance and therefore convergence problems. It therefore seems necessary to introduce a local modification of the upwind differencing scheme at the phase boundary.

(ii) Energy Imbalance during Two-Phase Flow Calculation

The second reason appears to be that during the two-phase flow calculation, the energy imbalance is generally large with peaks up to 10% of the input power. The reason for this discrepancy has been detected, although the problem is not yet completely solved.

The specific power released to the coolant is given by:

$$\frac{q}{v_f} = A\alpha \left(T_w - T_f\right) \quad [W/m^3] \,, \tag{3}$$

where

A = wetted surface of the power-source structure

T_f, T_w = coolant and wall temperatures

v_f = volume of the fluid

α = heat transfer coefficient.

The difference between two consecutive values of the specific power at iteration steps r, r+1 is given by

$$\frac{q^{r+1} - q^{r}}{v_f} = - \frac{A\alpha}{v_f} \left(T_f^{r+1} - T_f^{r} \right) \tag{4}$$

or, using

$dT = dh/c_p$ (h = coolant specific enthalpy):

$$\frac{q^{r+1} - q^{r}}{v_f} = - \frac{A\alpha}{v_f \cdot c_p} \left(h^{r+1} - h^{r} \right) . \tag{5}$$

When convergence of the solution of the energy equation

$$a_o \cdot h_o^{n+1} - \sum_{i=1}^{6} a_i \cdot h_i^{n+1} = b_o \tag{6}$$

is approached, both sides of Eq. (3) tend to vanish. It is therefore legitimate to add to the right and left sides of Eq. (4), the terms $\frac{A\alpha\, h^{r}}{v_f c_p}$ and $\frac{A\alpha\, h^{r+1}}{v_f c_p}$, respectively (these terms are added by modifying the coefficients b_o and a_o in Eq. 4). This artifice, which is used both in COMMIX-1 and COMMIX-2, provides the diagonal dominance to the matrix of coefficients of Eq. (4) and thus enhances the convergence rate.

Unlike the single phase flow case where the specific heat c_p is well defined, there is the difficulty of correctly defining c_p for the two-phase mixture. Replacing the liquid value of specific heat (which has been so far erroneously used) by

$$c_{pm} = c_{p\ell} \cdot (1 - x) + c_{pg} \cdot x \tag{7}$$

(where x is the thermodynamic quality, and the indices ℓ, g, and m refer to liquid, vapor, and mixture, respectively) has reduced the energy imbalance considerably. However, the problem has not yet been solved satisfactorily.

C.2 Two-Fluid Model

The following system of basic conservation equations forms the basis of the theoretical and numerical development of the two-fluid version (referred to herafter as COMMIX-2/4).

a. Continuity Equation

The continuity equations written separately for the vapor and liquid phases are

$$\frac{\partial \rho'_g}{\partial t} + \nabla \cdot \left(\rho'_g \bar{u}_g \right) = M , \tag{8}$$

and

$$\frac{\partial \rho_\ell'}{\partial t} + \nabla \cdot \left(\rho_\ell' \bar{u}_\ell\right) = -M \ , \tag{9}$$

where M is the coolant mass evaporating or condensing per unit time and unit volume; u_g, u_ℓ are the phase velocities, and ρ_g', ρ_ℓ' denote the macroscopic densities defined by

$$\rho_g' = \alpha \rho_g \ , \tag{10a}$$

and

$$\rho_\ell' = (1 - \alpha)\, \rho_\ell \ , \tag{10b}$$

with α = volumetric void fraction,

ρ_g = vapor microscopic density, and

ρ_ℓ = liquid microscopic density.

In a computational cell, both evaporation and condensation can be present with respective sources S_{me}, and S_{mc}. In this case, M represents the net mass balance given by

$$M = S_{me} - S_{mc} \ . \tag{11}$$

M is considered positive by net mass evaporation. The macroscopic density of the coolant is defined by

$$\rho_m = \alpha \rho_g + (1 - \alpha)\, \rho_\ell = \rho_g' + \rho_\ell' \tag{12}$$

b. Momentum Equations

The momentum equations for vapor and liquid phases are:

$$\frac{\partial \left(\rho_g' \bar{u}_g\right)}{\partial t} + \nabla \cdot \left(\rho_g' \bar{u}_g \bar{u}_g\right)$$

$$= M \left(\bar{u}_\ell - \bar{u}_g\right) - \alpha \nabla p + \bar{V}_g + \rho_g' \bar{g} + K\left(\bar{u}_\ell - \bar{u}_g\right) \tag{13}$$

and

$$\frac{\partial \left(\rho_\ell' \bar{u}_\ell\right)}{\partial t} + \nabla \cdot \left(\rho_\ell' \bar{u}_\ell \bar{u}_\ell\right)$$

$$= -M \left(\bar{u}_\ell - \bar{u}_g\right) - (1 - \alpha) \nabla p + \bar{V}_\ell + \rho_\ell' \bar{g} - K\left(\bar{u}_\ell - \bar{u}_g\right) \ , \tag{14}$$

where

V_g, V_ℓ = momentum density sources (in vapor and liquid) arising from viscous dissipation, and

K = drag function (to be specified).

c. Energy Equations

The energy equations for vapor and liquid phases are:

$$\rho_g' \left[\frac{\partial e_g}{\partial t} + \nabla \cdot (e_g \bar{u}_g) - e_g \nabla \cdot \bar{u}_g \right] = S_{ie_g} - S_{ic_g} + Q_g + R(T_\ell - T_g)$$

$$+ K(\bar{u}_\ell - \bar{u}_g)^2 + \nabla \cdot (K\alpha \nabla T_g) + V_{i_g} - p\nabla \cdot [\alpha \bar{u}_g + (1 - \alpha)\bar{u}_\ell] , \quad (15)$$

and

$$\rho_\ell' \left[\frac{\partial e_\ell}{\partial t} + \nabla \cdot (e_\ell \bar{u}_\ell) - e_\ell \nabla \cdot \bar{u}_\ell \right] = S_{ie_\ell} - S_{ic_\ell} + Q_\ell - R(T_\ell - T_g)$$

$$+ \nabla \cdot [K(1 - \alpha)\nabla T_\ell] + V_{i_\ell} , \quad (16)$$

where

S_{ie}, S_{ic} = Sources to internal energy arising from evaporation or condensation (including latent heat release or absorption),

Q_v, Q_ℓ = heat sources in vapor, liquid,

e_g, e_ℓ = specific internal energy of vapor and liquid,

R = heat exchange function, describing the transfer of heat between fields,

$K(\bar{u}_\ell - \bar{u}_g)^2$ = represents the effect of drag dissipation, which is assigned completely to the heating of vapor,

$p \nabla \cdot \alpha \bar{u}_g$ = work arising from vapor compression,

$p\nabla \cdot (1 - \alpha)\bar{u}_\ell$ = work associated with liquid acceleration, and

V_{ig}, $V_{i\ell}$ = energy sources arising from viscous absorption.

Combining the continuity and momentum equations (Eqs. 8 and 13 for the vapor phase, and Eqs. 9 and 14 for the liquid phase) with the usual ICE (Implicit Continuous Eulerian) technique, one derives the following system of algebraic equations for the velocity components (u, v, and w in the x, y, and z directions, respectively) of both phases:

$$a^{u}_{0\ell} \cdot u^{n+1}_{\ell,i+1,j,k} = \hat{u}_{2\ell} - (M + K)_{i+1/2,j,k} V_0 \left(u^{n+1}_{\ell} - u^{n+1}_{g}\right)_{i+1/2,j,k} - d_{2\ell}(1 - \alpha) \left(p^{n+1}_{2} - p^{n+1}_{0}\right)_{i+1,j,k} . \quad (17a)$$

$$a^{u}_{0g} \cdot u^{n+1}_{g,i+1,j,k} = \hat{u}_{2g} + (M + K)_{i+1/2,j,k} V_o \left(u^{n+1}_{\ell} - u^{n+1}_{g}\right)_{i+1/2,j,k} - d_{2g}\, \alpha \left(p^{n+1}_{2} - p^{n+1}_{0}\right)_{i+1,j,k} . \quad (17b)$$

$$a^{v}_{0\ell} \cdot v^{n+1}_{\ell,i,j+1/2,k} = \hat{v}_{4\ell} - (M + K)_{i,j+1/2,k} V_0 \left(v^{n+1}_{\ell} - v^{n+1}_{g}\right)_{i,j+1/2,k} - d_{4\ell}(1 - \alpha) \left(p^{n+1}_{4} - p^{n+1}_{0}\right)_{i,j+1,k} . \quad (17c)$$

$$a^{v}_{0g} \cdot v^{n+1}_{\ell,i,j+1/2,k} = \hat{v}_{4g} + (M + K)_{i,j+1/2,k} V_0 \left(v^{n+1}_{\ell} - v^{n+1}_{g}\right)_{i,j+1/2,k} - d_{4g}\, \alpha \left(p^{n+1}_{4} - p^{n+1}_{0}\right)_{i,j+1,k} . \quad (17d)$$

$$a^{w}_{0\ell} \cdot w^{n+1}_{\ell,i,j,k+1/2} = \hat{w}_{6\ell} - (M + K)_{i,j,k+1/2} V_0 \left(w^{n+1}_{\ell} - w^{n+1}_{g}\right)_{i,j,k+1/2} - d_{6\ell}(1 - \alpha) \left(p^{n+1}_{6} - p^{n+1}_{0}\right)_{i,j,k+1} . \quad (17e)$$

$$a^{w}_{0g} \cdot w^{n+1}_{\ell,i,j,k+1/2} = \hat{w}_{6g} + (M + K)_{i,j,k+1/2} V_o \left(w^{n+1}_{\ell} - w^{n+1}_{g}\right)_{i,j,k+1/2} - d_{6g}\, \alpha \left(p^{n+1}_{6} - p^{n+1}_{0}\right)_{i,j,k+1} . \quad (17f)$$

In Eq. 17 the indices i,j,k refer to the center node of a cell; n refers to the time level, V_0 is the fluid volume in the cell, M represents the mass of coolant vaporizing or condensing (considered positive by vaporization), K is a drag function (to be developed) between the phases, and the other coefficients a_0, d, and w are the COMMIX usual symbols (see Ref. 8).

Moreover, two discrete Poisson-like equations are obtained for describing the pressure distribution in the separated phases:

$$a^{\ell}_{0} \cdot p^{n+1}_{0} - \sum_{1}^{6} a^{\ell}_{i} \cdot p^{n+1}_{i} = b^{\ell}_{0} . \quad (18a)$$

$$a^{g}_{0} \cdot p^{n+1}_{0} - \sum_{1}^{6} a^{g}_{i} \cdot p^{n+1}_{i} = b^{g}_{0} . \quad (18b)$$

The coefficients of the Poisson-equations for the separated phases have been derived analytically, and are given hereafter for the liquid phase:

$$a_1^{\ell} = -\left[(1-\alpha)\,(\rho_{\ell}'A)\right]_{i-1/2} \cdot d_1^{\ell} \,. \tag{19a}$$

$$a_2^{\ell} = -\left[(1-\alpha)\,(\rho_{\ell}'A)\right]_{i+1/2} \cdot d_2^{\ell} \,. \tag{19b}$$

$$a_3^{\ell} = -\left[(1-\alpha)\,(\rho_{\ell}'A)\right]_{j-1/2} \cdot d_3^{\ell} \,. \tag{19c}$$

$$a_4^{\ell} = -\left[(1-\alpha)\,(\rho_{\ell}'A)\right]_{j+1/2} \cdot d_4^{\ell} \,. \tag{19d}$$

$$a_5^{\ell} = -\left[(1-\alpha)\,(\rho_{\ell}'A)\right]_{k-1/2} \cdot d_5^{\ell} \,. \tag{19e}$$

$$a_6^{\ell} = -\left[(1-\alpha)\,(\rho_{\ell}'A)\right]_{k+1/2} \cdot d_6^{\ell} \,. \tag{19f}$$

$$a_o^{\ell} = a_1^{\ell} + a_2^{\ell} + a_3^{\ell} + a_4^{\ell} + a_5^{\ell} + a_6^{\ell} \,. \tag{20}$$

$$b_o^{\ell} = -\frac{Vo}{\Delta t}\left(\rho_{o\ell}'^{\,n+1} - \rho_{o\ell}'^{\,n}\right) +$$

$$+\left[Vo\,\frac{\rho_{\ell}'A}{a^{u}_{o\ell}}\right]_{i+1/2} \cdot \left[(M+K)\,(u_{\ell}-u_g)\right]^{r+1}_{i+1/2} -$$

$$-\left[Vo\,\frac{\rho_{\ell}'A}{a^{u}_{o\ell}}\right]_{i-1/2} \cdot \left[(M+K)\,(u_{\ell}-u_g)\right]^{r+1}_{i-1/2} +$$

$$+\left[Vo\,\frac{\rho_{\ell}'A}{a^{v}_{o\ell}}\right]_{j+1/2} \cdot \left[(M+K)\,(v_{\ell}-v_g)\right]^{r+1}_{j+1/2} -$$

$$-\left[Vo\,\frac{\rho_{\ell}'A}{a^{v}_{o\ell}}\right]_{j-1/2} \cdot \left[(M+K)\,(v_{\ell}-v_g)\right]^{r+1}_{j-1/2} +$$

$$+\left[Vo\,\frac{\rho_{\ell}'A}{a^{w}_{o\ell}}\right]_{k+1/2} \cdot \left[(M+K)\,(w_{\ell}-w_g)\right]^{r+1}_{k+1/2} -$$

$$-\left[Vo\,\frac{\rho_{\ell}'A}{a^{w}_{o\ell}}\right]_{k-1/2} \cdot \left[(M+K)\,(w_{\ell}-w_g)\right]^{r+1}_{k-1/2} +$$

$$+ (\rho'A)_{i-1/2} \cdot \hat{u}_{1\ell} - (\rho'A)_{i+1/2} \cdot \hat{u}_{2\ell} + (\rho'A)_{i-1/2} \hat{v}_{3\ell} +$$

$$- (\rho'A)_{j+1/2} \hat{v}_{4\ell} + (\rho'A)_{k-1/2} \hat{w}_{5\ell} - (\rho'A)_{k+1/2} \hat{w}_{6\ell} \cdot \qquad (21)$$

It will be remarked that in case $\alpha = 0$, $\rho'_\ell = \rho_\ell$, $M = K = 0$, and Eqs. 19 through 21 reduce to the usual ones for the single-phase flow calculation.

Similar formulas for the vapor phase are obtained simply by replacing

$\rho'_\ell = (1 - \alpha)\rho_\ell$ with $\rho'_g = \alpha \rho_g$,

$(1 - \alpha)$ with α, and

$(M + K)$ with $-(M + K)$.

Assuming that a no-pressure gradient between the phases exists in a cell, Eqs. 20 and 21 can be summed to give a combined Poisson equation

$$a_0^\ell + a_0^g \; p_0^{n+1} - \sum_1^6 i \; a_i^\ell + a_i^g \; p_i^{n+1} = b_0^\ell + b_0^g \cdot \qquad (22)$$

Equation 22 can be solved numerically with the usual Poisson solver, thus yielding the coolant pressure distribution.

The system (17) can be solved algebraically, with respect to the velocity components, to obtain the following solution.

$$u^{n+1\,\ell}_{i+1/2,j,k} = \frac{XL2 \cdot XG3 + XL3 \cdot XG1}{XL1 \cdot XG1 - XL2 \cdot XG2} \cdot \qquad (23a)$$

$$v^{n+1\,\ell}_{i,j+1/2,k} = \frac{YL2 \cdot YG3 + YL3 \cdot YG1}{YL1 \cdot YG1 - YL2 \cdot YG2} \cdot \qquad (23b)$$

$$w^{n+1\,\ell}_{i,j,k+1/2} = \frac{ZL2 \cdot ZG3 + ZL3 \cdot ZG1}{ZL1 \cdot ZG1 - ZL2 \cdot ZG2} \cdot \qquad (23c)$$

$$u^{n+1\,g}_{i+1/2,j,k} = \frac{XL1 \cdot XG3 + XL3 \cdot XG2}{XL1 \cdot XG1 - XL2 \cdot XG2} \cdot \qquad (23d)$$

$$v^{n+1\,g}_{i,j+1/2,k} = \frac{YL1 \cdot YG3 + YL3 \cdot YG2}{YL1 \cdot YG1 - YL2 \cdot YG2} \cdot \qquad (23e)$$

$$w^{n+1\,g}_{i,j,k+1/2} = \frac{ZL1 \cdot ZG3 + ZL3 \cdot ZG2}{ZL1 \cdot ZG1 - ZL2 \cdot ZG2} \cdot \qquad (23f)$$

In Eq. 23, the symbols are defined as follows:

$$XL1 = {}^{w}a_{0\ell} + V_o(M + K)_{i+1/2,j,k} \cdot$$

$$XL2 = V_o(M+K)_{i+1/2,j,k} \cdot$$

$$XL3 = \hat{u}_{2\ell} - d_{2\ell}(1 - \alpha)\left(p_2^{n+1} - p_0^{n+1}\right).$$

$$XG1 = {}^{y}a_{0g} + V_o(M + K)_{i+1/2,j,k} \cdot$$

$$XG2 = XL2 .$$

$$XG3 = \hat{u}_{2g} - d_{2g}\,\alpha\left(p_2^{n+1} - p_0^{n+1}\right).$$

$$YL1 = {}^{v}a_{0\ell} + V_o(M + K)_{i,j+1/2,k} \cdot$$

$$YL2 = V_o(M+K)_{i,j+1/2,k} \cdot$$

$$YL3 = \hat{v}_{4\ell} - d_{4\ell}(1 - \alpha)\left(p_4^{n+1} - p_0^{n+1}\right).$$

$$YG1 = {}^{v}a_{0G} + V_o(M + K)_{i,j+1/2,k} \cdot$$

$$YG2 = YL2 .$$

$$YG3 = \hat{v}_{4g} - d_{4g}\,\alpha\left(p_4^{n+1} - p_0^{n+1}\right).$$

$$ZL1 = {}^{w}a_{0\ell} + V_o(M + K)_{i,j,k+1/2} \cdot$$

$$ZL2 = V_o(M+K)_{i,j,k+1/2} \cdot$$

$$ZL3 = \hat{w}_{6\ell} - d_{6\ell}(1 - \alpha)\left(p_6^{n+1} - p_0^{n+1}\right).$$

$$ZG1 = {}^{w}a_{0g} + V_o(M + K)_{i,j,k+1/2} \cdot$$

$$ZG2 = ZL2 .$$

$$ZG3 = \hat{w}_{6g} - d_{6g}\,\alpha\left(p_6^{n+1} - p_0^{n+1}\right).$$

So far, the following subroutines have been programmed:

XMOMIL : Calculates $\hat{u}_{2\ell}$ (≡ UHATL) and $d_{2\ell}$ (≡ DUØL) from the x-component of the liquid momentum.

YMOMIL : Calculates $\hat{v}_{4\ell}$ (≡ VHATL) and $d_{4\ell}$ (≡ DVØL).

ZMOMIL : Calculates $\hat{w}_{6\ell}$ (≡ WHATL) and $d_{6\ell}$ (≡ DWØL).

XMOMIG : Calculates $\hat{u}_{2g}$ (≡ UHATG) and d_{2g} (≡ DUØG).

YMOMIG : Calculates $\hat{v}_{4g}$ (≡ VHATG) and d_{4g} (≡ DvØG).

ZMOMIG : Calculates $\hat{w}_{6g}$ (≡ WHATG) and d_{6g} (≡ DWØG).

PEQNL : Computes the coefficients ACOFØL, ACOF1L .... ACOF6L, BCOFOL for the pressure Poisson equation derived from the liquid momentum equation.

PEQNG : Computes the coefficients ACFØG, ACOF1G.... ACOF6G, BCOFOG for the pressure equation derived from the vapor momentum equation.

REFERENCES

1. Physics of Reactor Safety Quarterly Report, July-September 1981, ANL-81-29, Vol. III, NUREG/CR-2181, Vol. III, p. 4.

2. Physics of Reactor Safety Quarterly Report, April-June 1981, ANL-81-29, Vol. II, NUREG/CR-2181, Vol. II, p. 4.

3. T. J. Scale, B. W. Spencer, J. J. Santori, W. C. Jeans, and R. L. McDaniel, "OPERA 15-Pin Sodium Expulsion Test," Trans. Am. Nucl. Soc., 43, pp. 495-497 (1982).

4. Physics of Reactor Safety Quarterly Report, January-March 1982, ANL-82-24, Vol. I, NUREG/CR-2774, Vol. I, pp. 2-5.

5. F. H. Harlow and J. E. Welch, Phys. Fluids 8 (1965), 2182, J. E. Welch, F. H. Harlow, J. P. Shannon, and B. J. Daly, "The MAC Method: A Computing Technique for Solving Viscous, Incompressible, Transient Fluid Flow Problems Involving Free Surfaces," Los Alamos National Laboratory report LA-3425 (1966).

6. B. D. Nichols, C. W. Hirt, and R. S. Hotchkiss, "Volume of Fluid (VOF) Method for the Dynamics of Free Boundaries," Los Alamos National Laboratory report, LA-8355 (1980).

7. A. R. Barbin and J. B. Jones, "Turbulent Flow in the Inlet Region of a Smooth Pipe," J. Basic Engineering, Trans. ASME, Vol. 85, p. 29 (1963).

8. H. M. Domanus, R. C. Schmitt, W. T. Sha, and V. L. Shah, "A New Implicit Numerical SI Solution Scheme in the COMMIX-1A Computer Program," ANL-83-64, NUREG/CR-3435 (September 1983).

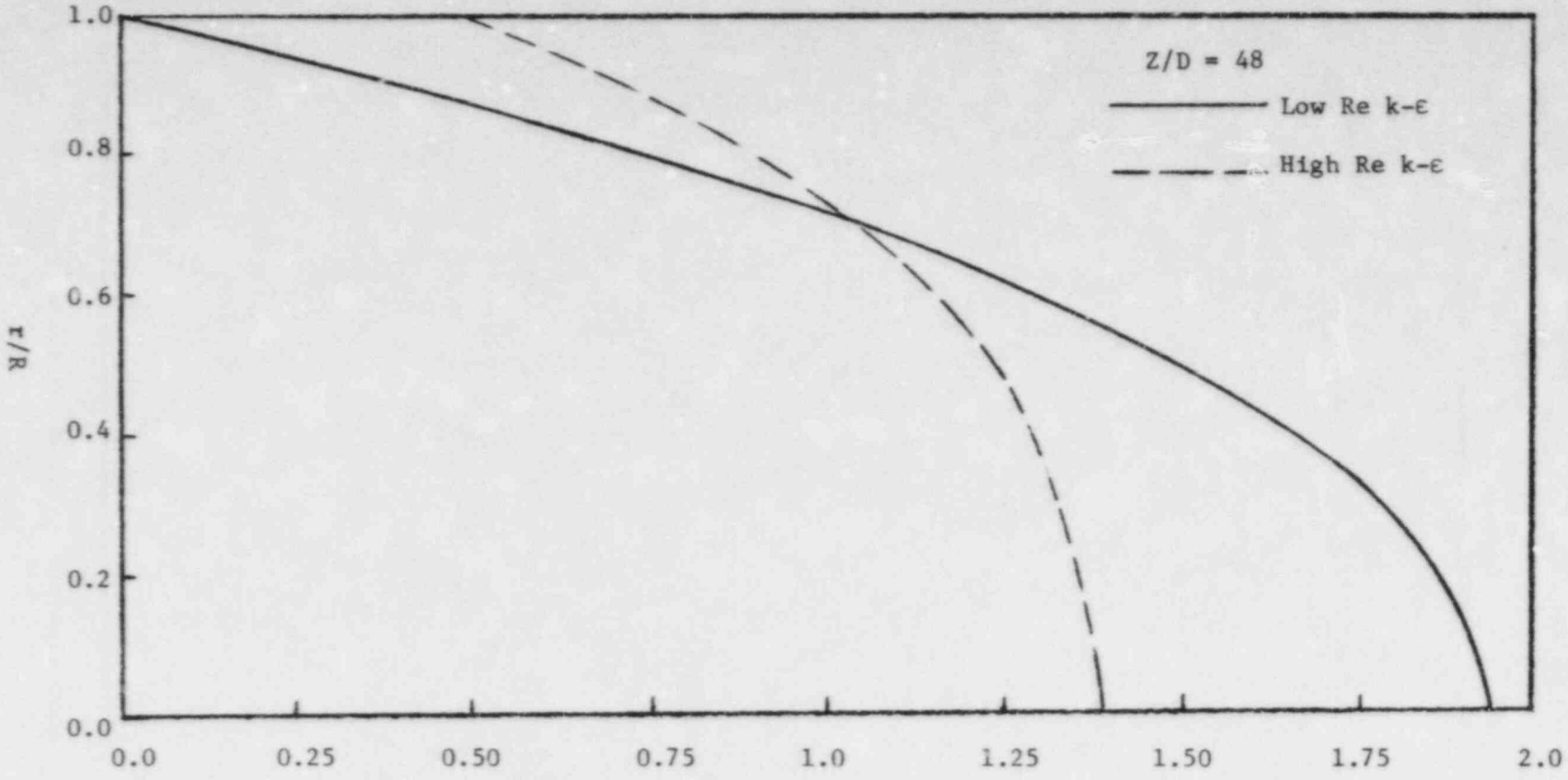

Fig. 1. Comparison of Axial Velocity Profile in a Pipe for Two Different Turbulent Models at Re = 1000

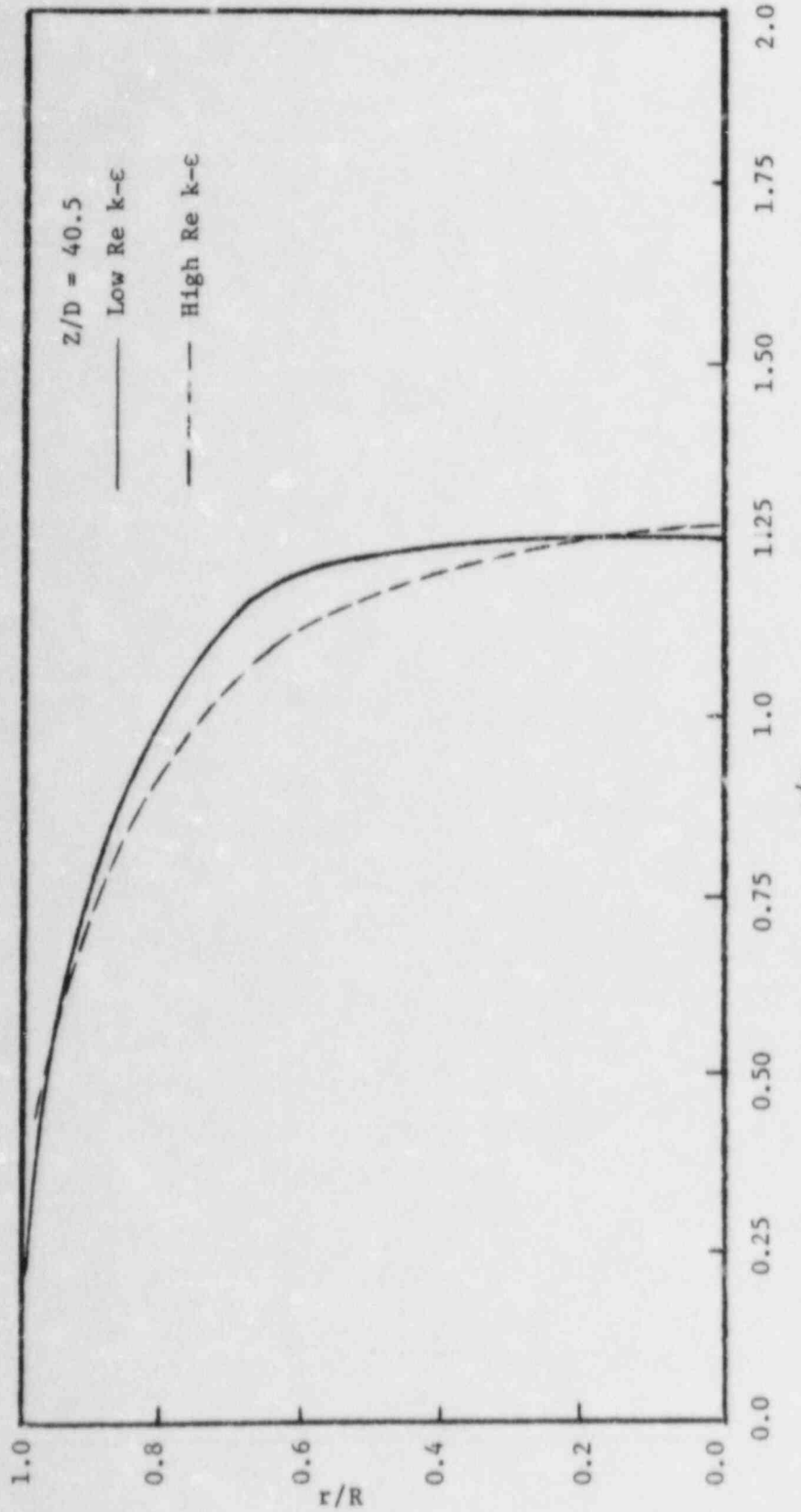

Fig. 2. Comparison of Axial Velocity Profile in a Pipe for Two Different Turbulent Models at Re = 2000

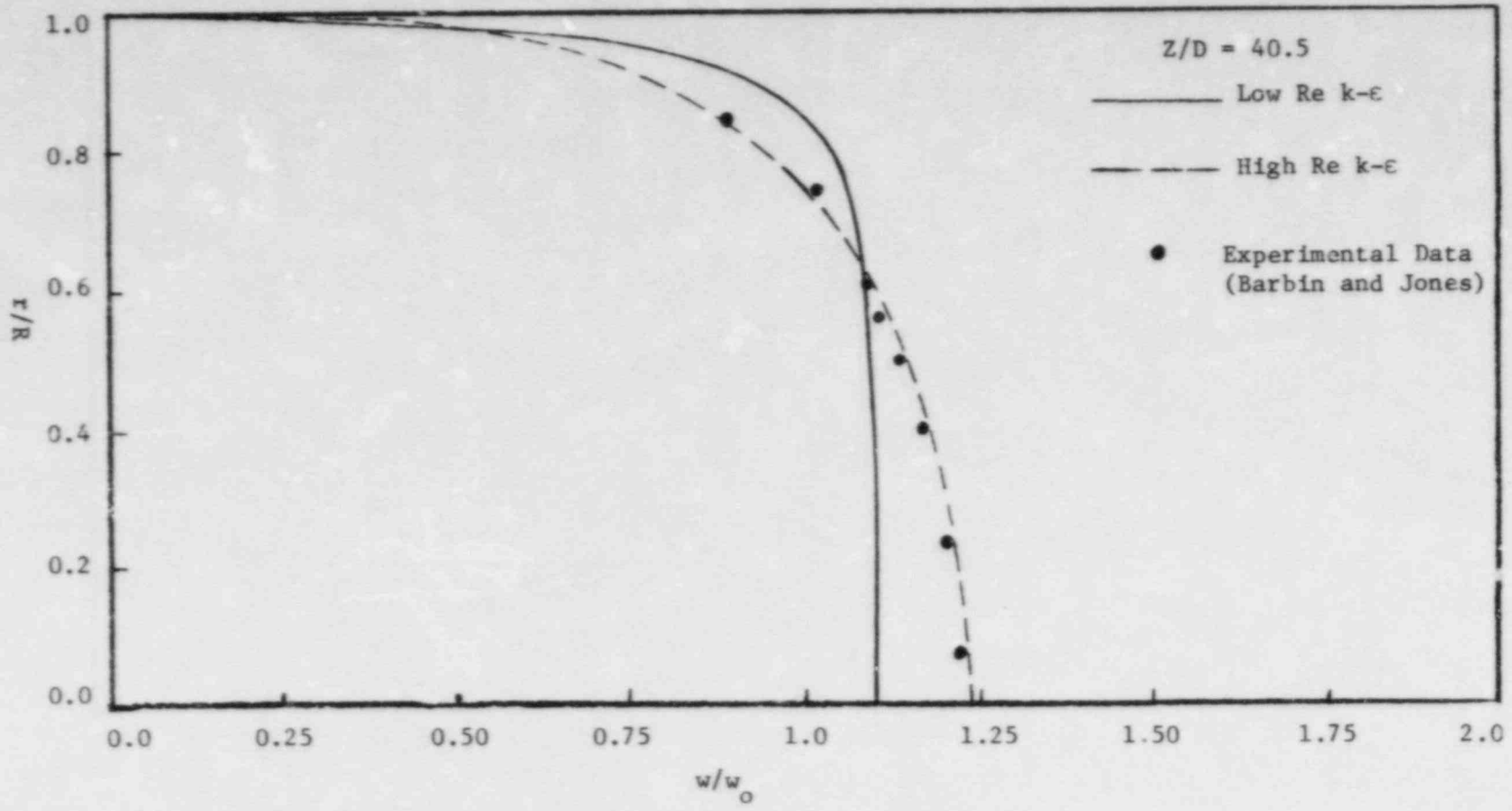

Fig. 3. Comparison of Axial Velocity Profile in a Pipe for Two Different Turbulent Models at Re = 3.38×10^5

Table 1. List of Functions used to Calculate Coolant Physical properties

FUNCTION		
NPROPS	:	To signal the presence of sodium or water properties.
CPLIQ	:	Coolant specific heat at constant pressure $C_{p\ell}$.
CPVAP	:	Vapor specific heat at constant pressure C_{pg}.
DRODHL	:	Derivative of liquid density with respect to enthalpy at constant pressure $(\partial_{\rho\ell}/\partial h)_{\rho}$.
DRODHV	:	Derivative of vapor density with respect to enthalpy at constant pressure $(\partial\rho_g/\partial h)_{\rho}$.
DRODPL	:	Derivative of liquid density with respect to pressure at constant enthalpy $(\partial\rho_\ell/\partial\rho)_h$.
DRODPV	:	Derivative of vapor density with respect to pressure at constant enthalpy $(\partial\rho_g/\partial\rho)_h$.
HLIQ	:	Enthalpy of subcooled and saturated liquid.
HVAP	:	Enthalpy of saturated and superheated vapor.
PSAT1	:	Coolant pressure p = p(T) at saturation temperature.
ROLIQ	:	Liquid coolant density at saturation ρ_ℓ.
ROVAP	:	Vapor density at saturation ρ_g.
SURTEN	:	Surface tension of liquid coolant σ.
THCLIQ	:	Thermal conductivity of liquid coolant K_ℓ.
THCVAP	:	Thermal conductivity of vapor K_v.
TLIQ	:	Temperature of liquid coolant $T_\ell = T_\ell(h, p)$.
TSAT11	:	Coolant saturation temperature $T_\ell = T_\ell(p)$.
TVAP	:	Coolant vapor temperature $T_g = T_g(h, p)$.
DPSADT	:	Derivative of saturation pressure with respect to temperature $[\partial\rho(T)/\partial T]$.
DHDPL	:	Derivative of liquid coolant enthalpy with respect to pressure at constant temperature $(\partial h_\ell/\partial\rho)_T$.
DHDPV	:	Derivative of vapor enthalpy with respect to pressure at constant temperature $(\partial h_v/\partial\rho)_T$.
VISLIQ	:	Liquid coolant viscosity $\mu_\ell = \mu_\ell(T)$.
VISVAP	:	Vapor viscosity $\mu_g = \mu_g(T)$.

Distribution for NUREG/CR-3804 Vol. I (ANL-84-35 Vol. I)

Internal:

E. S. Beckjord
C. E. Till
F. S. Onesto
R. Avery
P. B. Abramson
I. Bornstein/
A. B. Klickman
C. E. Dickerman
F. E. Dunn
R. A. Valentin/L. Baker
S. H. Fistedis
P. L. Garner
E. Gelbard
H. Henryson
H. H. Hummel (5)
Kalimullah
D. H. Lennox
L. G. LeSage
D. J. Malloy
A. P. Olson
P. Pizzica
F. G. Prohammer
D. Rose/A. J. Goldman/
J. F. Marchaterre
R. Sevy
J. J. Sienicki
W. J. Sturm
B. J. Toppel
J. B. van Erp
D. Weber
H. M. Domanus
V. L. Shah
B. C-J. Chen
W. T. Sha
F. I. Amundson/
S. G. Carpenter
M. J. Lineberry
D. H. Shaftman
A. Travelli
ANL Contract File
ANL Patent Dept.
ANL Libraries (2)
TIS Files (3)

External:

USNRC, Washington, for distribution per R7 (250)
DOE-TIC, Oak Ridge (2)
Manager, Chicago Operations Office, DOE
Applied Physics Division Review Committee:
P. W. Dickson, Jr., Clinch River Breeder Reactor Project, Oak Ridge, Tenn. 37830
W. E. Kastenberg, U. California, Los Angeles, Calif. 90024
K. D. Lathrop, Los Alamos National Lab., P. O. Box 1663, Los Alamos, N. M. 87545
N. J. McCormick, U. Washington, Seattle, Wash. 98195
D. A. Meneley, Ontario Hydro, 700 University Ave., Toronto, Canada M5G 1X6
J. E. Meyer, Massachusetts Inst. Technology, Cambridge, Mass. 02139
A. E. Wilson, Idaho State U., Pocatello, Id. 83209
Components Technology Division Review Committee:
D. J. Anthony, General Electric Co., Schenectady, N. Y. 12345
A. A. Bishop, U. Pittsburgh, Pittsburgh, Pa. 15261
B. A. Boley, Northwestern U., Evanston, Ill. 60201
F. W. Buckman, Consumers Power Co., 1945 Parnall Rd., Jackson, Mich. 49201
R. Cohen, Purdue U., West Lafayette, Ind. 47907
E. E. Ungar, Bolt, Beranek and Newman Inc., 50 Moulton St., Cambridge, Mass. 02138
J. Weisman, U. Cincinnati, Cincinnati, O. 45221
C. Erdman, Texas A&M U., College Station, Tex. 77843
R. Lancet, Atomics International, P. O. Box 309, Canoga Park, Calif. 91304
K. O. Ott, Purdue U., West Lafayette, Ind. 47907

NRC FORM 335 (11-81)

U.S. NUCLEAR REGULATORY COMMISSION

BIBLIOGRAPHIC DATA SHEET

1. REPORT NUMBER (Assigned by DDC)
ANL 84-35 Vol. I
NUREG/CR-3804 Vol. I

4. TITLE AND SUBTITLE (Add Volume No., if appropriate)
Physics of Reactor Safety Quarterly Report
January-March 1984

2. (Leave blank)

3. RECIPIENT'S ACCESSION NO.

7. AUTHOR(S)
Applied Physics Division
Components Technology Division

5. DATE REPORT COMPLETED
MONTH: May YEAR: 1984

9. PERFORMING ORGANIZATION NAME AND MAILING ADDRESS (Include Zip Code)
Argonne National Laboratory
9700 S. Cass Avenue
Argonne, IL 60439

DATE REPORT ISSUED
MONTH: June YEAR: 1984

6. (Leave blank)

8. (Leave blank)

12. SPONSORING ORGANIZATION NAME AND MAILING ADDRESS (Include Zip Code)
Division of Reactor Safety Research
Office of Nuclear Regulatory Research
U.S. Nuclear Regulatory Commission
Washington, D.C. 20555

10. PROJECT/TASK/WORK UNIT NO.

11. FIN NO.
A2015
A2045

13. TYPE OF REPORT
Quarterly (Physics of Reactor Safety)

PERIOD COVERED (Inclusive dates)
January-March 1984

15. SUPPLEMENTARY NOTES

14. (Leave blank)

16. ABSTRACT (200 words or less)

This quarterly progress report summarizes work done during the months of January-March 1984 in Argonne National Laboratory's Applied Physics and Components Technology Divisions for the Division of Reactor Safety Research in the U.S. Nuclear Regulatory Commission. The work in the Applied Physics Division includes reports on reactor safety modeling and assessment by members of the Reactor Safety Appraisals Section. Work on reactor core thermal-hydraulics is performed in ANL's Components Technology Division, emphasizing 3-dimensional code development for LMFBR accidents under natural convection conditions. An executive summary is provided including a statement of the findings and recommendations of the report.

17. KEY WORDS AND DOCUMENT ANALYSIS

17a. DESCRIPTORS

LMFBR Safety
Core Disruptive Accident Analysis
CRBR Licensing
Reactor Core Thermal Hydraulics
Natural Convection Core Cooling

17b. IDENTIFIERS/OPEN-ENDED TERMS

18. AVAILABILITY STATEMENT
Unlimited

19. SECURITY CLASS (This report)
unclassified

21. NO. OF PAGES

20. SECURITY CLASS (This page)
unclassified

22. PRICE
$

NRC FORM 335 (11-81)